ISSN 1392-1207. MECHANIKA. Vol. 31, No. 3, 2025: 169–181

Enhancing Fracture Assessment of Pipe Girth Welds with Root Cracks

Xiatong WU*, Han ZHANG*, Shengsi WU*, Pengchao CHEN, Hao WANG*, Xiaoben LIU*****

**China University of Petroleum-Beijing, National Engineering Laboratory for Pipeline Safety/MOE Key Laboratory of Petroleum Engineering/Beijing Key Laboratory of Urban Oil and Gas Distribution Technology, Beijing 102249, China*
***Pipechina Research Institute, Langfang 065000, China*
****China University of Petroleum-Beijing, National Engineering Laboratory for Pipeline Safety/MOE Key Laboratory of Petroleum Engineering/Beijing Key Laboratory of Urban Oil and Gas Distribution Technology, Beijing 102249, China, E-mail: xiaobenliu@cup.edu.cn (Corresponding Author)*

https://doi.org/10.5755/j02.mech.37831

1. Introduction

Girth welds, being vulnerable links in pipeline transportation systems, inevitably exhibit welding defects stemming from construction environments and welding quality, among other factors. These defects make them especially susceptible to failure under non-design axial tensile loads [1, 2]. In recent years, numerous incidents worldwide involving high-strength pipeline steels failing due to girth weld crack initiation have highlighted the critical importance of girth weld cracks in affecting the safe operation of oil and gas pipelines [3, 4].

The Failure Assessment Diagram (FAD), originally developed by the Central Electricity Generating Board in the UK, is the predominant method for assessing the integrity of structures with crack-type defects. Widely adopted by various defect assessment standards globally, including API 579 [5], BS 7910 [6], and GB/T 19624 [7], FAD is integral to ensuring structural safety. However, the advent of high-grade pipelines has highlighted a critical limitation in current assessment methodologies, including FAD, regarding their inability to accurately account for the effects of weld strength mismatch in pipe girth welds. This oversight significantly restricts the method's efficacy in evaluating crack fracture behaviour accurately, underscoring the need for enhanced assessment strategies that consider the complexities introduced by weld strength mismatch.

In response to the challenges posed by weld strength mismatch, Lei et al. [8] proposed to consider the heterogeneous girth welds as an equivalent homogeneous structure and derived an equivalent stress-strain relation for girth welds. Building upon this foundation, Lei and Ainsworth [9] further refined the approach by developing a technique for constructing failure evaluation curves based on the equivalent stress-strain relation, specifically tailored for crack assessment at weld positions. This innovative method has been successfully integrated into BS 7910, representing a significant milestone to incorporate weld strength matching considerations into the evaluation of cracked defects within pipeline girth welds.

Researchers have extended the application of such homogenization method to the fracture assessment of subsea pipelines, addressing the complexities of various service conditions. Souza et al. [10] developed a technique to compute the *J*-integral for under-matched pipes featuring circumferential girth weld cracks. This approach uniquely incorporates equivalent material parameters and considers the limit load of strength-mismatched structures, offering a refined analysis of fracture potential under specific welding conditions. Zhao et al. [11] applied the same method for calculating the *J*-integral, specifically focusing on ovalized pipeline girth welds under bending loads. Further contributions to the field have been made by Kim [12, 13], Tkaczyk [14], Jia [15], and Li [16], who explored the precise calculation of the limit load in homogeneous pipelines using the FAD method. These studies proposed adjustments to load forms and material characteristics, aiming to improve the prediction of failure rates. Through these various applications, the homogenization method has proven to be a versatile and effective tool in enhancing the reliability of fracture assessments across a wide range of welding conditions and structural complexities.

In recent years, finite element analysis (FEA) has emerged as a novel and effective means for the safety evaluation of structures containing defects [10, 17, 18]. By simulating structures with defects using finite element analysis, it becomes possible to fully consider the mechanical properties of materials, the boundary conditions of structures, and the forms of loads to obtain the stress distribution near the defect location and fracture assessment parameters. These parameters are then compared with existing technical standards to determine the acceptability of the defect [19, 20]. The latest edition of the BS 7910 fracture assessment procedure exemplifies this approach, utilizing numerical analysis to establish accurate failure assessment curves for defect evaluation, thereby providing standardized support for this method of defect assessment.

The underlying cause that impacts the failure evaluation result of pipeline girth weld root crack defects is the methodology used for calculating the load ratio of the failure assessment diagram [21]. However, the accuracy of the load ratio calculation hinges on the reference stress and the limit load capacity of the girth weld. This study introduces an advanced FEA model to enhance the precision in evaluating in pipeline girth weld root crack defects. By characterizing the crack driving force for root cracks in girth welds, the failure assessment curve with the highest evaluation accuracy can be established. Then, based on the traditional failure assessment curve, the correction factor is introduced to established a refined method for calculating the reference stress and limit load of pipeline girth welds. This method builds upon the limit load calculation model of girth welds. Furthermore, a predictive formula for the correction factor has been formulated, drawing upon finite element simulation results and accounting for various factors such as crack size, pipeline

diameter-thickness ratio, yield-tensile strength ratio and weld strength matching factors. Overall, by leveraging these advancements, this study aims to provide guidance for the girth weld root cracks evaluations in engineering applications, ultimately bolstering the integrity and reliability of critical infrastructure systems within the pipeline industry.

2. FAD Construction for Girth Welded Pipes

2.1. Equivalent stress-strain relation for weldment

In the context of heterogeneous welded structures, such as pipeline girth welds characterized by strength mismatching, establishing failure assessment curves poses unique challenges. Lei and Ainsworth proposed a novel approach wherein the limit load of different materials is equivalently weighted to transform a strength-mismatched structure into a homogeneous material structure [9]. This transformation leverages the true stress-strain relationship of the equivalent homogeneous structure to construct the failure assessment curve. For strength-mismatched girth welds, the stress-strain curve of the equivalent homogeneous material is derived from the constitutive relationships of the parent metal and weld metal, along with their respective limit loads, as demonstrated in the following equation:

$$\sigma^M\left(\varepsilon_{pl}\right)=\frac{\left(\frac{P_L^M}{P_L^P}-1\right)\sigma^W\left(\varepsilon_{pl}\right)}{\left(m-1\right)}+\frac{\left(m-\frac{P_L^M}{P_L^P}\right)\sigma^P\left(\varepsilon_{pl}\right)}{\left(m-1\right)}, \quad (1)$$

where $\sigma^M(\varepsilon_{pl})$, $\sigma^W(\varepsilon_{pl})$ and $\sigma^P(\varepsilon_{pl})$ are the plastic constitutive relations of the equivalent homogeneous material, weld metal, and parent metal, respectively; P_L^M and P_L^P are the corresponding limit loads of equivalent material and parent metal; m is the strength matching factor between the weld metal and parent metal. For calculating the limit load of girth welds with surface cracks under tensile loads, Kim et al. proposed a method based on finite element analysis for high strength matching welds [22]:

$$\frac{P_L^M}{P_L^B}=\begin{cases}min\left(m,\dfrac{1}{1-a/B}\right), & 0\le\psi\le\psi_1\\ min\left(\dfrac{24\left(m-1\right)}{25}\left(\dfrac{\psi_1}{\psi}\right)+\dfrac{\left(m+24\right)}{25},\ \dfrac{1}{1-a/B}\right), & \psi_1\le\psi\end{cases}, \quad (2)$$

where ψ is the crack geometric parameter defined as:

$$\psi=\frac{\left(B-a\right)}{h}+5\left[cos\left(\frac{\theta}{2}\right)-\frac{sin\,\theta}{2}\right]. \quad (3)$$

Here, θ is the half circumferential angle of crack, and h denotes the weld width. Parameter ψ_1 is defined as:

$$\psi_1=exp\left[-\frac{2\left(m-1\right)}{5}\right]. \quad (4)$$

For an under-matched girth weld

$$\frac{P_L^M}{P_L^B}=\begin{cases}m & 0\le\psi\le1.5\\ 1-\dfrac{1.5\left(1-m\right)}{\psi} & 1.5\le\psi\end{cases}. \quad (5)$$

2.2. General failure assessment curve construction

The BS 7910 standard provides a stress-based failure assessment procedure for homogenous structures, the failure assessment curve can be written as:

$$f\left(L_r\right)=\left(\frac{E\varepsilon_{ref}}{L_r\sigma_y}+\frac{L_r^{\,3}\sigma_y}{2E\varepsilon_{ref}}\right)^{-0.5} \quad \text{for} \quad L_r\le L_{r,max}, \quad (6)$$

where E is the Young's modulus; L_r is the load ratio; ε_{ref} is the strain corresponding to the reference stress according to the true stress and strain of the material; σ_y is the yield strength of the material. However, the above formula is derived under the assumption of homogeneous material properties. For the pipe girth weld joint with heterogeneous material properties, the equivalent stress-strain relation established in Eq. (1) is used.

The assessment point coordinates are determined by the load ratio L_r and toughness ratio K_r. The load ratio L_r is determined by the following equation:

$$L_r=\frac{\sigma_{ref}}{\sigma_y^M}=\frac{P}{P_L^M}, \quad (7)$$

where σ_{ref} is the reference stress applied on the structure; σ_y^M is the yield strength of equivalent material; P is the external axial loading applied on the pipeline; P_L^M is the limit load of the girth weld joint. The BS 7910 standard recommends employing the Kastner formula [6] to describe the relationship between the reference stress within the pipeline under an external axial load, which is expressed as follows:

$$P=2\pi R_m B\sigma_{ref}\frac{\left(1-\frac{a}{B}\right)\left[\pi-\left(\frac{c}{R}\right)\left(\frac{a}{B}\right)\right]}{\pi\left(1-\frac{a}{B}\right)+2\left(\frac{a}{B}\right)\sin\left(\frac{c}{R}\right)}, \quad (8)$$

where R_m is the radius of the pipe; B is the pipe wall thickness; a is the crack depth and c is the half length of the crack.

The toughness ratio K_r is determined by the following equation:

$$K_r=\sqrt{\frac{J_e}{J_{mat}}}, \quad (9)$$

where J_e the elastic portion of J integral, obtained from the J integral from the elastic analysis; J_{mat} is the fracture toughness of weld metal from the elastic-plastic analysis.

3. Finite Element Analysis Model

3.1. Geometry of the pipe girth weld with an inner surface crack

The pipeline girth weld featuring a circumferential localized internal surface crack is depicted in Fig. 1. Positioned at the centreline of the weld, the crack exhibits a canoe shape, which closely resembles the actual crack shape [23]. Its geometric attributes are defined by the crack depth a and the crack length $2c$.

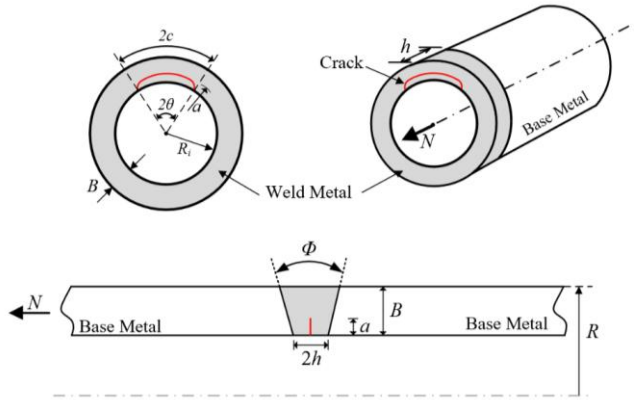

Fig. 1 Geometry of the pipe girth weld with an inner surface crack

The geometric dimensions of the pipeline are established based on the D1422 mm pipeline specification, where the pipeline diameter is 1422 mm. To explore the influence of the pipe diameter-thickness ratio, various wall thicknesses of 21.4 mm, 25.7 mm and 30.8 mm are examined. For crack depth characterization, the dimensionless parameter a/B is varied across values of 0.2, 0.3, 0.4 and 0.5, while the dimensionless parameter $c/\pi R$, representing crack length, is varied across values of 0.01, 0.015, 0.02 and 0.025. The weld root width is set as 8 mm, representing typical automated girth welds. Notably, misalignment at the weld joint has not been accounted for in the current model. A summary of the geometric parameters is presented in Table 1.

To leverage the geometric symmetry of the structure, a half pipeline model is constructed with a localized internal surface crack at the girth weld centreline by utilizing the finite element software ABAQUS. Symmetric constraint boundary conditions are imposed on the symmetric surfaces of the pipeline to accurately capture the structural behaviour. Notably, the crack surface remains free without any boundary conditions applied. Additionally, two reference points are created at each end of the pipe. The pipe ends are then coupled to these reference points. One reference point is constrained in all directions to simulate the fixed end of the pipe, while the motion of the other reference point is controlled by displacement to apply an axial tensile load on the pipe. This setup enables the accurate simulation of loading conditions and structural response, facilitating comprehensive analysis of the crack behaviour within the pipeline.

In this FEA model, the total length of the pipeline is set to six times the diameter of the pipe, ensuring a representative simulation domain [24, 25]. Quadratic brick elements with reduced integral (C3D20R) are employed to discretize the model, providing efficient and accurate representation of the structural behaviour. The element size varies based on the distance from the crack surface, with a smallest element size of 5 mm and the largest element size of 100 mm. To accurately simulate the crack front and characterize stress singularities, a spider web type mesh with wedge-shaped degenerate elements is utilized. Furthermore, local mesh refinement with an element size of 0.1 mm is implemented near the crack tip to ensure computational accuracy in stress and strain fields. The FEA model, depicted in Fig. 2, has been developed with consideration of numerous parameter combinations. To streamline the process and reduce time costs associated with establishing FEA models, a parameterized modelling Python script has been developed, enabling efficient and systematic generation of FEA models across various scenarios.

Table 1

Geometric parameters for FEA

Diameter D, mm	Wall thickness B, mm	Crack depth ratio a/B	Crack length ratio $c/\pi R$	Weld width $2h$, mm
1422	21.4, 25.7, 30.8	0.2, 0.3, 0.4, 0.5	0.01, 0.015, 0.02, 0.025	8

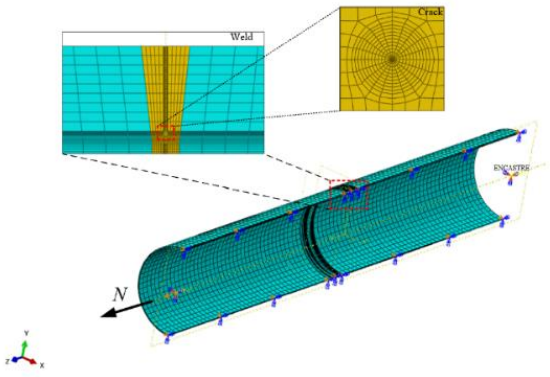

Fig. 2 FEA model for the crack driving force calculation

In this analysis, the J integral serves as a crucial metric for characterizing the crack driving force. ABAQUS facilitates automatic output of J integral results based on predefined contour paths. To accurately capture the J integral values, ten contours are established through the spider web mesh. It's important to note that the J integral may vary along the crack length direction. To ensure consistency in the analysis, the J integral at the symmetry plane position along the crack length direction has been identified as the maximum crack driving force. Although the path independence principle of the J integral suggests that the selected contour should not influence the result, practical observations indicate higher error in the J integral along the 1st contour path. Conversely, the errors associated with the remaining J integrals are less than 5%. Given these considerations, the 10th J integral is selected as the output for this study, ensuring robust and reliable characterization of the crack

driving force while minimizing potential errors associated with contour selection.

3.2. Material properties

For the weld and parent metal, the constitutive relations are modeled by using the Ramberg-Osgood formula [26, 27]:

$$\varepsilon = \frac{\sigma}{E} + \alpha \frac{\sigma_y}{E}\left(\frac{\sigma}{\sigma_y}\right)^n, \tag{10}$$

$$\alpha = \frac{E\varepsilon_y}{\sigma_y} - 1, \tag{11}$$

$$n = \frac{1}{0.3(1-\lambda)}, \tag{12}$$

where E is the Young's modulus, set as 210 GPa for both the weld and parent metal; σ_y is the yield strength, ε_y is the corresponding yield strain; α is the parameter controls the yield offset, which can be determined by Eq. (11); n is the hardening factor which can be calculated based on the yield to tensile ratio λ, as shown in Eq. (12). The relevant FEM model material parameters are shown in Table 2. Four values of the yield to tensile ratio λ are examined: 0.75, 0.8, 0.85 and 0.9. For the parent metal, the yield strength is varied across three levels: 500 MPa, 550 MPa and 600 MPa. Meanwhile, the weld metal's strength matching factor, is explored across five scenarios: 0.8, 0.9, 1.0, 1.1 and 1.2. These diverse material parameter combinations facilitate a comprehensive investigation into the structural response under varied loading conditions and material compositions.

3.3. FEA model validation

3.3.1. Crack driving force calculation

To validate the established model, the FEA results were compared with those derived from the linear elastic stress intensity factor (SIF) calculation method for local circumferential cracks. It's important to note that the SIF formula provided by BS 7910 is applicable only under the assumption of linear elasticity. Therefore, purely elastic material model was implemented in the FEA analysis to ensure compatibility. Three cases of crack depth were selected for comparative calculations, with detailed parameters provided in Table 3. This comparative analysis serves to assess the fidelity of the FEA model and its alignment with established analytical methods, enhancing confidence in the accuracy of the structural analysis.

A comparison between the FEA results and the calculations from BS 7910 is illustrated in Fig. 3. For a crack depth ratio of 0.1, the results from both methods align closely, exhibiting an error of only 2.3%. This agreement

Table 2

Material parameters for FEA models

Elastic Parameters		Plastic Parameters		
Elastic modulus E, MPa	Poisson's ratio ν	Yield strength σ_y^B, MPa	Yield-tensile strength ratio λ	Matching factor m
210000	0.3	500, 555, 600	0.75, 0.8, 0.85, 0.9	0.8, 0.9, 1.0, 1.1, 1.2

Table 3

Table of analyses for verification of FEM model crack driving force

Geometric parameters	Material properties	Axial load
B = 21.4 mm a/B = 0.1, 0.3, 0.5 $c/\pi R$ = 0.025	E = 210000 MPa ν = 0.3	P= 1.2 σ_y^M

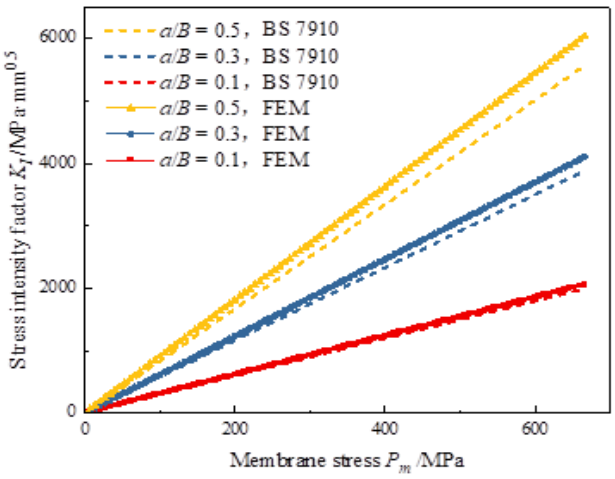

Fig. 3 Comparison of FEM and BS 7910 K_I results

diminishes as the crack depth increases. With a crack depth ratio of 0.3, the discrepancy between the two methods widens to 4.1%. At a depth ratio of 0.5, the average relative error escalates to 6.7%. Such disparities can be attributed to differences in crack shape assumptions between the current FEA model and the BS 7910 standard. While BS 7910 presumes a semi-elliptical crack shape, the shape considered in this study resembles a canoe-like shape, which more accurately reflects the real crack shape observed in pipelines [23, 28]. The semi-elliptical shape features a non-uniform crack depth distribution along its length, achieving its maximum depth solely at the center. Hence, the two shapes exhibit similarity when the crack is shallow and its length relatively large. However, as the crack depth increases, the distinction between these two shapes becomes increasingly significant.

3.3.2. Verification for limit load calculation

Since the structural limit load is needed to establish the FAD, the established finite element model needs to be

verified for the limit load calculation. For this purpose, the limit load obtained from FEA simulation were compared with those obtained using the BS 7910 formula. The pipe diameter used for model verification is 1422 mm with the wall thickness of 21.4 mm. The crack length ratio is 0.025, and three crack depth ratios are selected as 0.1, 0.3 and 0.5. Elastic-perfectly plastic model is used for both the pipe parent metal and the weld. The yield strength of the parent metal is 555 MPa, and the weld strength matching factor is set as 1.0 and 1.2. The relevant parameters are shown in Table 4.

The BS 7910 standard suggests to calculate the structural limit load using the Kastner formula as described in Eq. (8). It assumes that structural failure occurs when the local reference stress σ_{ref} reaches the material's yield strength. At this point, the external tensile loading applied is the limit load that the structure can withstand. Therefore, the limit load of the pipeline can be calculated by plugging the equivalent yield strength of the girth weld structure obtained by Eq. (1) into Eq. (8). Such analytical solutions are used as the reference value for the FEA simulation results.

Table 4

Parameters of the limit load validation

Geometric parameter	Material parameter	Strain Level
D = 1422 mm B = 21.4 mm a / B = 0.1, 0.3, 0.5 c /πR = 0.025	E = 210000 MPa ν = 0.3 σ_y^B = 555 MPa m = 1.0, 1.2	ε_{nom} = 5%

Based on the FEA model outlined in the previous section, the reaction force at the loading reference point is extracted to determine the limit load of pipeline. By utilizing an elastic-perfectly plastic model in FEA simulation, the reaction force progressively increases to its maximum value and stabilizes as the displacement applied. Consequently, the plateau value of the reaction force is considered as the limit load. The comparison of analytical and FEA calculation results is shown in Table 5.

By comparing the limit load obtained via the analytical Kastner formula and the FEA simulation, the maximum relative error for the even-matched girth weld is 1.83%, and the maximum relative error for the over-matched girth weld is 2.57%. Such comparison reveals that under the equal strength matching condition, the Kastner solution is consistently lower than the FEA results, demonstrating the conservative nature of the Kastner solution. Under high strength matching conditions, however, the Kastner solution exhibits slightly aggressive results compared to FEA results when the crack depth ratios are 0.1 and 0.3. Across all validation scenarios, the maximum relative error between the two methods is 2.57%, with the minimum being -0.32%, which verifies the FEA model accuracy in limit load calculations.

Table 5

Comparison of FEA and Kastner formula for limit load

Strength matching factor	Crack depth ratio a/B	Kastner formula, 10^7N	FEA results, 10^7N	Relative Error, %
Even-matched weld m = 1.0	0.1	5.184	5.222	0.73
	0.3	5.078	5.171	1.82
	0.5	4.915	5.005	1.83
Over-matched weld m = 1.2	0.1	5.333	5.226	-2.01
	0.3	5.239	5.222	-0.32
	0.5	5.087	5.217	2.57

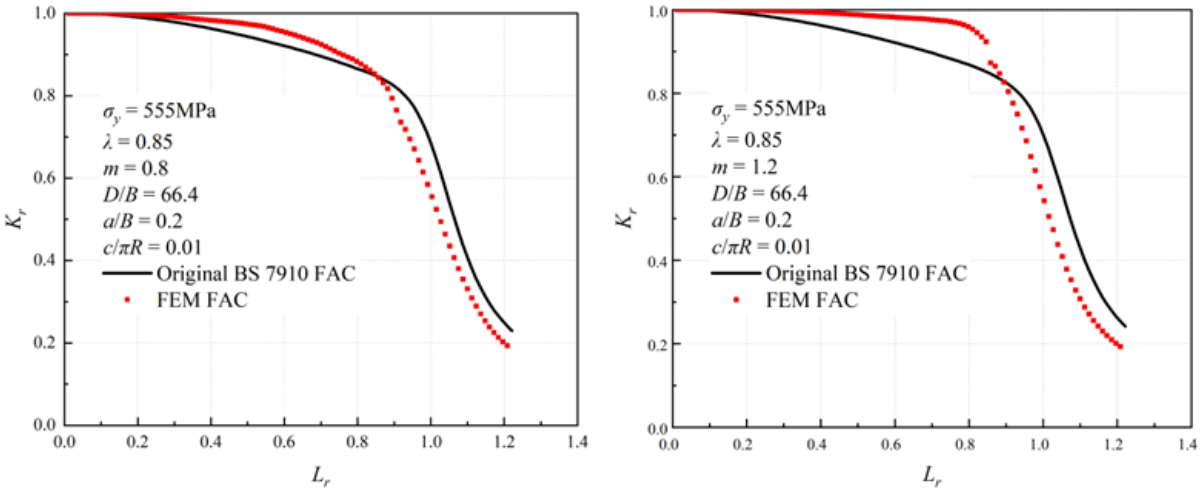

a b

Fig. 4 Stress-based failure assessment diagram established by FEA and BS 7910: a – m = 0.8, b – m = 1.2

4. Optimization for the Failure Assessment of Pipeline Girth Welds

Fig. 4 presents the failure assessment curves for pipeline girth welds under two specific working conditions, juxtaposing results from the BS 7910 analytical formula against those derived from FEA simulations. The BS 7910-based failure assessment curve is illustrated with a black line, whereas the FEA simulation results are marked with red dots, each representing the girth weld's safety limit under varying load conditions. In an ideal scenario, where the assessment methodology achieves perfect accuracy, points from FEA simulations would coincide with the analytical failure assessment curve. However, Fig. 4 indicates a divergence in this ideal alignment. Specifically, it shows that the two failure assessment curves would cross each other as the load ratio approximately equals 0.9.

Before such crossing, the FEA-derived assessment points consistently fall outside the BS 7910 curve, indicating a more conservative assessment within this range, henceforth referred to as the "conservative zone". In contrast, after the crossing, the assessment points are located within the boundary of the failure assessment curve, signalling a shift towards a less conservative assessment in what is identified as the "non-conservative zone". This discrepancy underscores the necessity to adjust the assessment method for improved accuracy and reliability across all load conditions.

In certain loading scenarios, the assessment outcomes maybe non-conservative due to constraints in calculating the load ratio within the assessment method. Ainsworth [21] suggested that, in deriving the general failure assessment curve, the dimensionless factor ratio $h_1(n) / h_1(n=1)$ is set to one through the selection of an appropriate limit load calculation model, as illustrated:

$$\frac{J_p}{J_e} = \alpha \frac{h_1(n)}{h_1(n=1)} \left(\frac{P}{P_L} \right)^{n-1} . \tag{13}$$

The sensitivity of the dimensionless factor $h_1(n) / h_1(n=1)$ to the prevailing limit load calculation methods is notable, and assuming constancy in this factor can be challenging to satisfy. Consequently, direct utilization of the current limit load calculation model may yield inaccurate assessment outcomes. To address this challenge, optimization of the existing limit load model can be achieved by drawing insights from the optimization reference stress method introduced by KIM and Budden [29]. The optimized reference load is defined as:

$$P_L^{op} = \gamma P_L , \tag{14}$$

where γ is the correction factor. Now Eq. (13) can be written as:

$$\frac{J_p}{J_e} = \alpha \left[\frac{h_1(n)}{h_1(n=1)} \left(\frac{P_L^{op}}{P_L} \right)^{n-1} \right] \left(\frac{P}{P_L^{op}} \right)^{n-1} . \tag{15}$$

By introducing the correction factor, the optimized reference stress calculation equation can be rewritten as:

$$\sigma_{ref}^{op} = \frac{P}{P_L^{op}} \sigma_y = \frac{1}{\gamma} \sigma_y . \tag{16}$$

Then Eq. (8) can be further written with the optimized reference stress:

$$f(L_r) = \left(\frac{E\varepsilon_{ref}^{op}}{\sigma_{ref}^{op}} + \frac{L_r^{\,3} \sigma_{ref}^{op}}{2E\varepsilon_{ref}^{op}} \right)^{-0.5} , \tag{17}$$

where ε_{ref}^{op} is now the strain corresponding to the optimized reference stress. The optimized load ratio could also be calculated using the optimized reference stress:

$$L_r^{\,op} = \frac{\sigma_{ref}^{op}}{\sigma_y} = \frac{P}{P_L^{op}} = \frac{1}{\gamma} L_r , \tag{18}$$

In the failure assessment diagram, the correction factor γ represents the ratio of L_r corresponding to the BS 7910-based failure assessment curve under the same K_r condition to L_r corresponding to the FEA evaluation curve. This ratio varies with the load level. To minimize the non-conservativeness of the current method, the maximum value

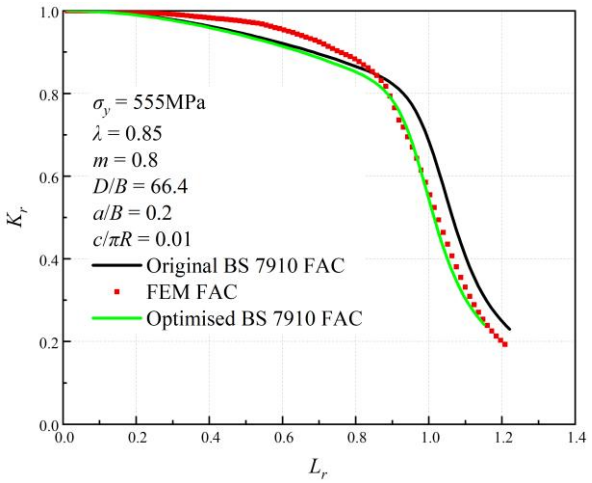

a

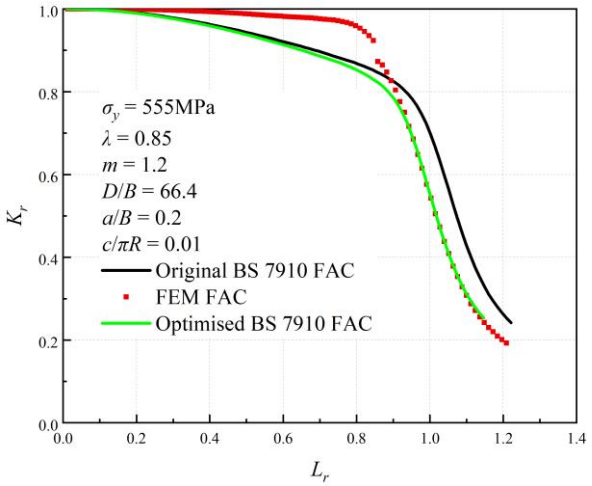

b

Fig. 5 Optimized failure assessment curves: a – $m = 0.8$, b – $m = 1.2$

across all load levels is selected as the correction factor γ for a specific working condition. This ensures that the optimized standard assessment curves align with the finite element curves. However, in cases where the FEA evaluation curve falls outside the BS 7910 curve, indicating inherent conservativeness in the standard method, no correction is needed in this scenario.

By performing above optimization procedures, the corresponding γ values for strength matching factors of 0.8 and 1.2 are 1.0498 and 1.0545, respectively. Consequently, assessment curves derived from the optimized method and the original method are illustrated in Fig. 5. It is apparent that the optimized assessment curve aligns with the original assessment curve within the conservative zone. While, for the non-conservative portion, optimized assessment curve shifts to coincide with the FEA derived assessment points, indicating a noteworthy enhancement in the conservativeness and accuracy of assessing girth weld cracks under high-stress conditions. Hence, the optimized assessment curve remains conservative in all domains.

5. Parametric Analysis of Correction Factor

This section aims to enhance the applicability of the proposed optimization method by analyzing the correlations between the correction factor γ and some key engineering parameters. The parameters subjected to analysis include the weld strength matching factor, yield strength, yield-tensile strength ratio, crack depth ratio, crack length ratio, and pipe diameter-thickness ratio.

5.1. Influence of yield-tensile strength ratio and crack depth ratio

In the comparative analysis between the failure assessment curves derived from the BS 7910 standard methodology and those obtained through FEA, as depicted in Fig. 6, variations are observed across different crack depth ratios, ranging from 0.2 to 0.5, under various yield-tensile strength ratios. Fig. 6 reveals that while the influence of crack depth on the failure assessment curve is minimal, the yield-tensile strength ratio significantly affects the curve's morphology. Notably, within the non-conservative zone, an increase in the yield-tensile strength ratio precipitates a steeper decline in the curves, illustrating a reduced deformation capacity in materials exhibiting higher yield-tensile strength ratios.

This observation is critical, as it highlights the conservative nature of the FEA-derived curves, which tend to lie outside the FEA curves when $L_r > 0.9$, signalling a

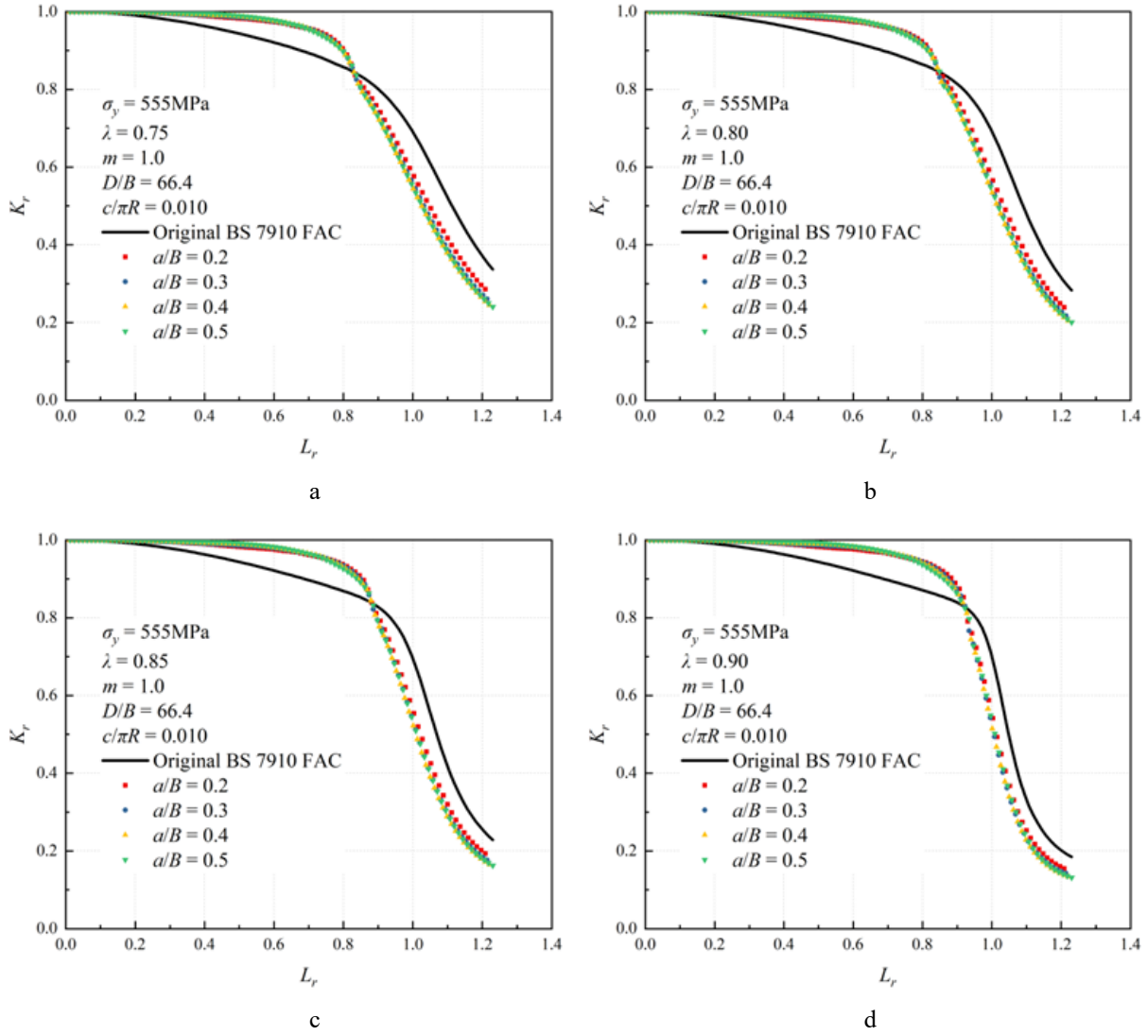

Fig. 6 Effect of crack depth ratio and yield-tensile strength ratio on failure assessment curve under equal strength matching conditions: a – λ = 0.75, b – λ = 0.80, c – λ = 0.85, d – λ = 0.90

potential non-conservativeness in the latter at this specific phase. The determination of the correction factor γ for varying parameters ensued, employing the methodology delineated in the preceding section, aiming to rectify this discrepancy and enhance the assessment's accuracy.

Fig. 7 elucidates the variation in the correction factor in response to changes in both crack depth ratio and yield-tensile strength ratio. It substantiates that the yield-tensile strength ratio exerts a more pronounced influence on the value of γ compared to the crack depth ratio, corroborating the observations regarding failure assessment curve variations presented in Fig. 7. Specifically, Fig. 7, a illustrates the impact of the crack depth ratio on γ. Within a constant yield-tensile strength ratio, the correction factor initially increases and subsequently decreases as the crack depth ratio rises, delineating a quadratic relationship. Conversely, Fig. 7, b delineates how the yield-tensile strength ratio affects γ. Holding the crack depth ratio constant, γ exhibits a monotonic decrease with an escalating yield-tensile strength ratio, indicative of a linear relationship. These findings underscore the critical roles that both crack depth and yield-tensile strength ratios play in determining the correction factor, thereby influencing the accuracy of the failure assessment.

5.2. Influence of strength matching factor and crack length ratio

Fig. 8 delineates the failure assessment curves with the crack length ratio ranging from 0.01 to 0.025 across various strength matching factors. This comparison reveals that for all examined strength matching factors, an increased crack length ratio correlates with a decreased conservativeness in the assessment outcomes produced by the existing method. Specifically, as the load ratio escalates, the assessment curve is first breached by the largest crack length ratio, signalling the transition of the existing assessment methods into the non-conservative phase. Subsequently, assessment points corresponding to smaller crack length ratios progressively intersect with the assessment curve, illustrating the intuitive notion that longer cracks are more prone to failure in such assessments.

Furthermore, an increase in the strength matching factors leads to a discernible flattening of the FEA assessment curves prior to intersecting with the original FAC, thereby encompassing a more extensive area within the diagram. This phenomenon suggests that girth welds possessing higher strength matching factors exhibit enhanced resistance to failure under plastic deformation, indicating a superior capability to withstand failure-inducing conditions. This analysis underscores the intricate interplay between crack length ratios, strength matching factors, and their collective impact on the conservativeness and reliability of pipeline failure assessments.

Fig. 9, a illustrates the relationship between the correction factor γ and the crack length ratio, demonstrating a monotonic increase in γ as the crack length ratio rises for a given strength matching factor.

Conversely, Fig. 9, b explores the influence of the strength matching factor on the correction factor γ, revealing a more complex behaviour. For a constant crack length ratio, γ initially decreases, then increases upon further escalation in the strength matching factor, with a notable local minimum at a matching factor of approximately 1.0. This point signifies the condition of an evenly matched girth weld, characterized by minimal disparity between FAC obtained through the BS 7910 and the FEA. The proximity of these curves suggests that an evenly matched girth weld, which may be perceived as a more homogeneous structure, offers enhanced assessment accuracy compared to a more heterogeneous girth weld configuration.

The observed trends imply that while both crack length ratio and strength matching factor significantly influence γ, the crack length ratio exerts a more pronounced impact. This indicates the correction factor is more sensitive to the physical characteristics of the crack, reinforcing the importance of these parameters in refining the accuracy of failure assessments. The nuanced relationship between γ and the strength matching factor underscores the intricacy of material properties in determining the reliability of the assessment, especially highlighting the improved precision in evaluating evenly matched girth welds.

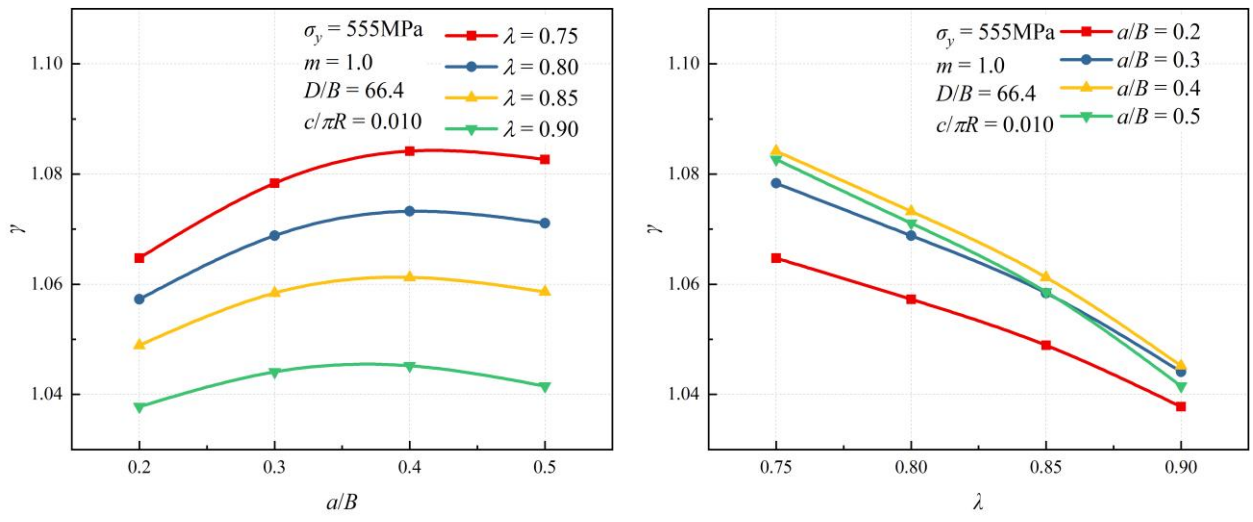

a b

Fig. 7 Effect of crack depth ratio and yield-tensile strength ratio on correction factor: a – effect of a/B on correction factor γ, b – effect of λ on correction factor γ

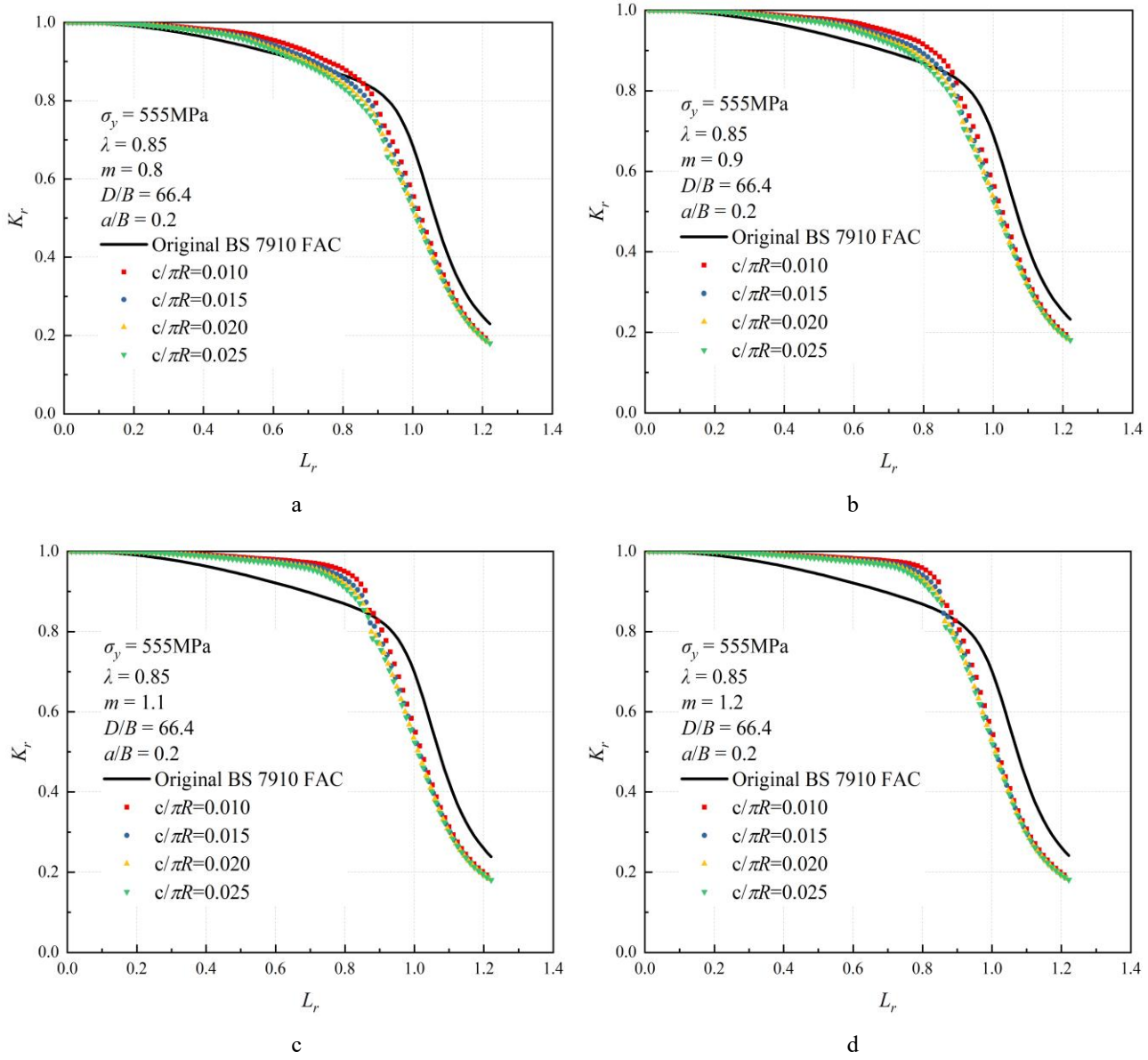

Fig. 8 Effect of crack length ratio and strength matching factor on FAC: a - $m = 0.8$, b - $m = 0.9$, c - $m = 1.1$, d - $m = 1.2$

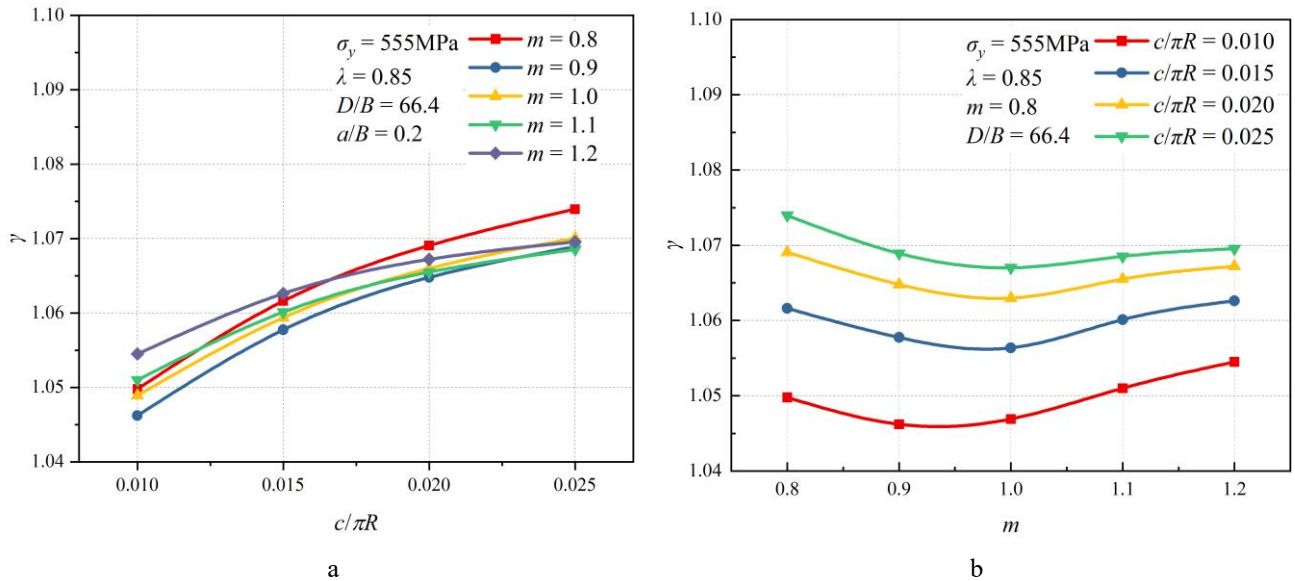

Fig. 9 Effect of crack length ratio and strength matching factor on correction factor: a – effect of $c/\pi R$ on correction factor γ, b – effect of m on correction factor γ

5.3. Influence of pipe diameter-thickness ratio and yield strength

Fig. 10 illustrates the failure assessment curves for pipes under varying diameter-thickness ratios and yield strength values, offering insights into the effects of these parameters on the assessment's outcomes. Three specific diameter-thickness ratios of 46.2, 55.3 and 66.4 are examined to elucidate their impact on the FAC morphology. Concurrently, the analysis spans yield strengths of 500 MPa, 555 MPa and 600 MPa, encapsulating the conventional yield strength range for X80 pipeline steel.

The FAC reveals a consistent pattern: among the different yield strengths evaluated, the configuration with the largest diameter-thickness ratio breaches the failure assessment curve initially. As the load ratio escalates, the curves corresponding to smaller diameter-thickness ratios sequentially intersect the failure assessment curve. This trend signifies that pipes with a smaller diameter and thicker walls exhibit enhanced resistance against plastic deformation leading up to failure, highlighting the critical role of geometric dimensions in determining pipeline robustness.

Contrastingly, the failure assessment curves exhibit negligible variation across the range of yield strengths analyzed. This observation suggests that within the specific range of yield strengths considered, the material's yield strength has a limited influence on the overall shape and position of the failure assessment curves. Such findings underscore the paramount importance of geometric factors, particularly the diameter-thickness ratio, in influencing pipeline failure assessments, while also indicating a relative insensitivity of the assessment outcomes to variations in yield strength within the bounds of typical X80 pipeline steel properties.

Fig. 11, a presents the impact of the pipe diameter-thickness ratio on the correction factor γ, demonstrating a consistent monotonic increase in γ with an increase in the diameter-thickness ratio for a given yield strength. Remarkably, the values of γ remain largely consistent across different yield strengths, suggesting that variations in yield strength exert minimal influence on γ.

Moreover, Fig. 11, b elucidates the effect of yield strength on γ, revealing that γ remains relatively constant as the yield strength ranges from 500 MPa to 600 MPa, irrespective of the fixed diameter-thickness ratio. Consequently, given the negligible influence of yield strength on γ, it is deemed unnecessary to incorporate yield strength into the subsequent fitting of the prediction formula for the correction factor γ. Instead, emphasis should be placed on other influential parameters, such as the diameter-thickness ratio, to refine and optimize the accuracy of the assessment method.

5.4. Predictive model for correction factor

The FAC of the BS 7910 standard have undergone modification through finite element analysis, resulting in the generation of a comprehensive database comprising 960 valid datasets encompassing various parameter combinations. Leveraging this dataset, an analysis and calculation of the influencing factors have been conducted to elucidate the sensitivity factors governing the correction factor γ.

The initial phase of the analysis involved the identification of univariate patterns through systematic examination. Subsequently, an appropriate formula structure was

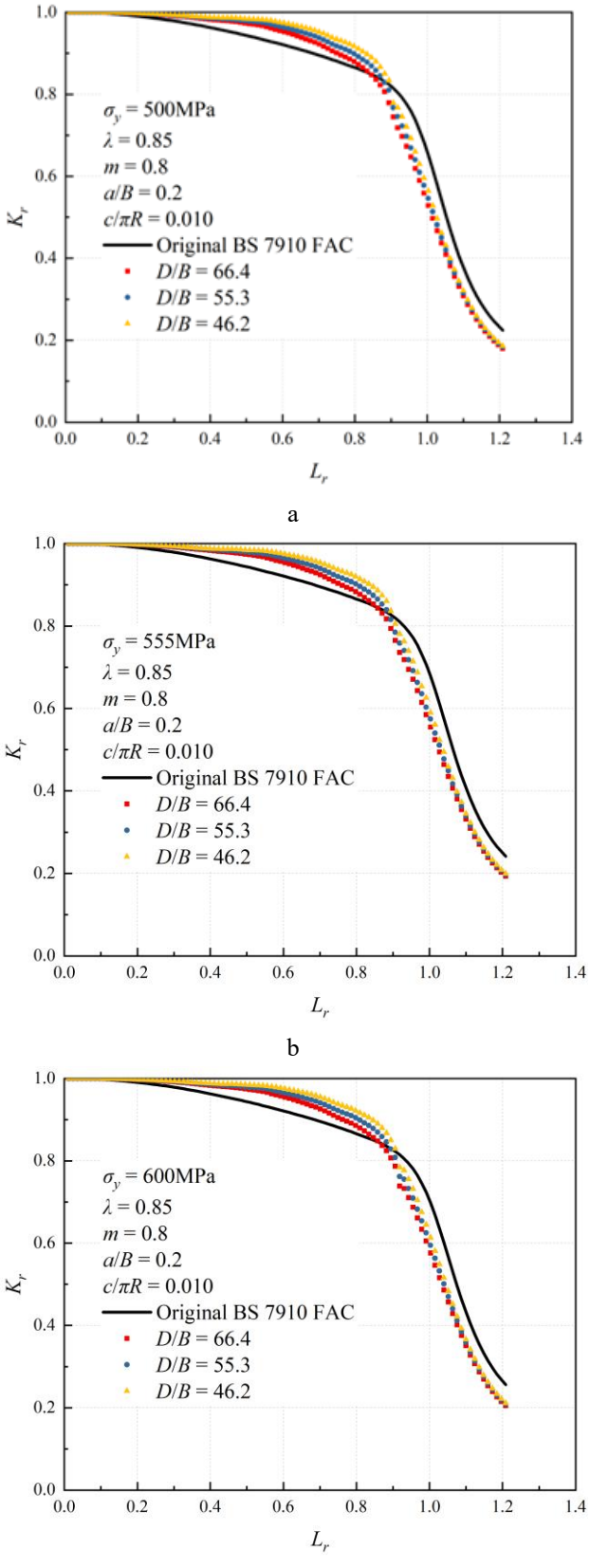

Fig. 10 Effect of pipe diameter-thickness ratio and yield strength on FAC: a – σ_y = 500 MPa, b – σ_y = 555 MPa, c – σ_y = 600 MPa

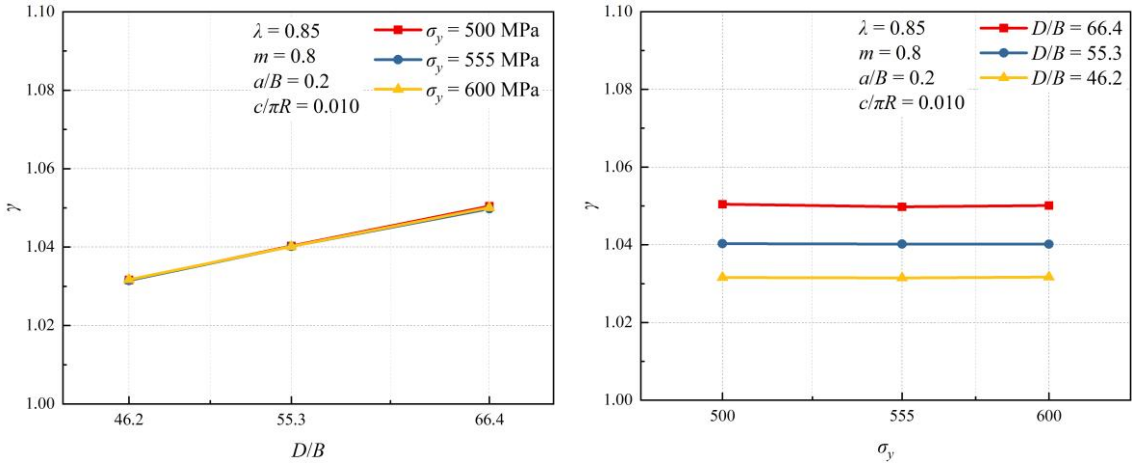

a b

Fig. 11 Effect of pipe diameter to thickness ratio and parent metal yield strength on correction factor: a – effect of D/B on correction factor γ, b – effect of σ_y on correction factor γ

discerned to encapsulate the complex relationship between the correction factor and its influencing factors. Finally, employing MATLAB's multivariate nonlinear regression function, the unknown coefficients within the formula were meticulously fitted to the dataset, culminating in the derivation of the predictive formula for the correction factor. The formulated predictive formula for the correction factor is as follows. The fitting coefficient values are given in Table 6. Based on the parameter values used in the finite element analysis, the applicable range of the above predictive formula is:

$0.2 \le a/B \le 0.5$; $0.01 \le c/\pi R \le 0.5$; $46.2 \le D/B \le 66.4$; $0.75 \le \lambda \le 0.9$; $0.8 \le m \le 1.2$.

In accordance with Eq. (19), the correction factor computed using the prediction formula is compared with the results obtained from finite element calculations, as depicted in Fig. 12. The comparison reveals that the majority of comparison points fall within the 1% relative error

$$
\begin{aligned}
&\eta = 1 + g_1\left(\frac{a}{B},\frac{c}{\pi R},\frac{D}{B}\right) + g_2\left(\frac{a}{B},\frac{c}{\pi R},m\right) + g_3\left(\frac{a}{B},\frac{c}{\pi R},\lambda\right) + g_4\left(m,\lambda\right),\\
&g_1\left(\frac{a}{B},\frac{c}{\pi R},\frac{D}{B}\right) = \left(\beta_1\left(\frac{c}{\pi R}\right)^{-1} + \beta_2\right)\left(\frac{a}{B}\right)^2 + \left(\beta_3\left(\frac{c}{\pi R}\right)^{-1} + \beta_4\right)\left(\frac{a}{B}\right) + \left(\beta_5\left(\frac{D}{B}\right)^{-1} + \beta_6\right),\\
&g_2\left(\frac{a}{B},\frac{c}{\pi R},m\right) = \left(\beta_7\left(\frac{a}{B}\right)^{\beta_8} + \beta_9\right)\left(\beta_{10}\left(\frac{c}{\pi R}\right) + \beta_{11}\right)(m-1),\\
&g_3\left(\frac{a}{B},\frac{c}{\pi R},\lambda\right) = \left(\beta_{12}\left(\frac{a}{B}\right)^2 + \beta_{13}\left(\frac{a}{B}\right) + \beta_{14}\left(\frac{c}{\pi R}\right) + \beta_{15}\right)(\lambda + \beta_{16}),\\
&g_4\left(m,\lambda\right) = \left(\beta_{17}\left(m-1\right) + \beta_{18}\right)\lambda^{\left(\beta_{19}(m-1)+\beta_{20}\right)}.
\end{aligned}
\tag{19}
$$

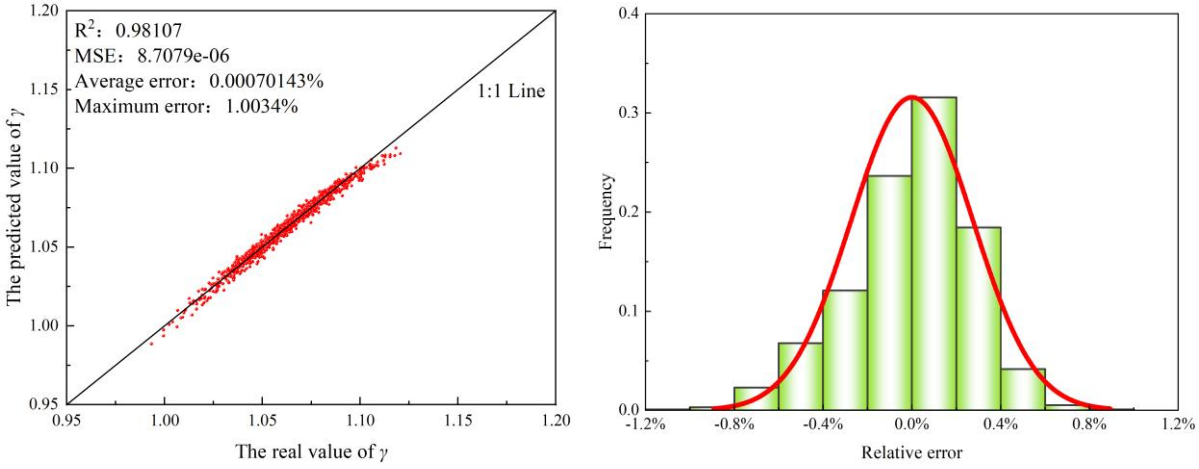

a b

Fig. 12 Accuracy analysis of the predictive formula for correction factor: a – 1:1 graph of γ true and predicted values, b – relative error distribution diagram

Table 6

Fitting coefficients for prediction model of γ

	β_{5i+1}	β_{5i+2}	β_{5i+3}	β_{5i+4}	β_{5i+5}
$i = 0$	0.0073	-1.0639	-0.0035	0.6299	-2.4987
$i = 1$	0.0935	2.5019	1.2546	-0.7393	3.5103
$i = 2$	0.0630	1.7693	-1.6115	-7.0207	0.4059
$i = 3$	-0.8144	0.1619	-0.1019	-2.9299	3.9618

boundary, highlighting the high accuracy achieved by the prediction model incorporating γ. This outcome attests to the efficacy and reliability of the proposed prediction model, affirming its capability to accurately predict the correction factor across diverse parameter combinations.

6. Conclusions

While the FAD serves as a widely utilized method for assessing defects in the pipeline industry, accurately evaluating root centreline cracks in pipeline girth welds remains a persistent challenge. To address this issue, the equivalent homogenization method offers an innovative approach, thereby enabling the construction of FAD for girth weld structures. However, the theoretical derivation of such a general failure assessment curve structured, as defined in BS 7910, hinges upon the selection of a limiting load calculation model or reference stress calculation method that satisfies specific assumptions. Meeting these criteria in all scenarios proves challenging and may introduce limitations to the accuracy of evaluations. To overcome these challenges and enhance evaluation accuracy, a numerical simulation model of a pipeline weld with root centreline crack is developed to characterize the crack driving force in high-grade pipeline girth welds. By constructing an accurate FAC based on finite element result, the traditional FAC is modified. In the process of modification, an optimized calculation method is proposed for determining the reference stress and limit load of pipeline girth welds afflicted with root cracks. This method effectively integrates considerations of weld strength matching into the failure assessment process, thereby enhancing the precision of evaluating root centreline crack defects within strength-mismatched girth welds subjected to axial tensile load.

Acknowledgements

This research has been co-financed by:

1. Key Science and Technology Project of Ministry of Emergency Management of the People's Republic of China (Grant No. 2024EMST090903);

2. National Key R&D Program of China (Grant No. 2022YFC3070100);

3. Young Elite Scientists Sponsorship Program by Beijing Association for Science and Technology (Grant No. BYESS2023261).

References

1. **Cao, Y.G.; Chang, Q.; Zhen, Y.** 2022. Numerical simulation of fracture behavior for the pipeline with girth weld under axial load, Engineering Failure Analysis 136: 106221. https://doi.org/10.1016/j.engfailanal.2022.106221.
2. **Yi, D.; Xiao, Z. M.; Idapalapati, S.; Kumar, S. B.** 2012. Fracture analysis of girth welded pipelines with 3D embedded cracks subjected to biaxial loading conditions, Engineering Fracture Mechanics 96: 570-587. https://doi.org/10.1016/j.engfracmech.2012.09.005.
3. **Yang, F.P.; Cheng F.; Zhang, H. B.** et al. 2022. Failure case and full-scale test of oil and gas pipeline girth weld, Oil Pipes and Instruments 8(04): 80-84. https://doi.org/10.19459/j.cnki.61-1500/te.2022.04.017.
4. **Li, L. Y.; Niu, X. W.; Liu, X. G.** et al. 2021. Current situation and prospect of ECA technology for high grade oil and gas pipelines, Transactions of Materials and Heat Treatment 42(07): 20-28. https://doi.org/10.13289/j.issn.1009-6264.2021-0025.
5. Fitness-For-Service API 579-1/ASME FFS-1. 2016. Washington, DC: American Petroleum Institute.
6. BS 7910: 2019 Guide on Methods for Assessing the Acceptability of Flaws in Metallic Structures. London: British Standard Limited. 535p.
7. GB/T 19624-2019. Safety assessment of in-service pressure vessels containing defects. The Standardization Administration of the People's Republic of China.
8. **Lei, Y.; Ainsworth, R. A.** 1997. A *J* integral estimation method for cracks in welds with mismatched mechanical properties, International Journal of Pressure Vessels and Piping 70(3): 237-245. https://doi.org/10.1016/S0308-0161(96)00035-X.
9. **Hertele, S.; O'Dowd, N. P.; van Minnebruggen, K.; Verstraete, M.; De Waele, W.** 2015. Fracture mechanics analysis of heterogeneous welds: Numerical case studies involving experimental heterogeneity patterns, Engineering failure analysis 58: 336-350. https://doi.org/10.1016/j.engfailanal.2015.07.007.
10. **Souza, R. F.; Ruggieri, C.; Zhang, Z.** 2016. A framework for fracture assessments of dissimilar girth welds in offshore pipelines under bending, Engineering Fracture Mechanics 163: 66-88. https://doi.org/10.1016/j.engfracmech.2016.06.011.
11. **Zhao, H. S.; Lie, S. T.; Zhang, Y.** 2018. Fracture assessment of mismatched girth welds in oval-shaped clad pipes subjected to bending moment, International Journal of Pressure Vessels and Piping 160: 1-13. https://doi.org/10.1016/j.ijpvp.2017.12.002.
12. **Kim, Y.; Zhu, X. K.; Chao, Y. J.** 2001. Quantification of constraint on elastic-plastic 3D crack front by J-A_2 three-term solution, Engineering Fracture Mechanics 68(7): 895-914. https://doi.org/10.1016/S0013-7944(00)00134-X.
13. **Kim, Y.; Chao Y. J.; Zhu, X. K.** 2003. Effect of specimen size and crack depth on 3D crack-front constraint for SENB specimens, International Journal of Solids and Structures 40(23): 6267-6284. https://doi.org/10.1016/S0020-7683(03)00392-5.

14. **Tkaczyk, T.; O'Dowd, N. P.; Nikbin, K.** 2009. Fracture Assessment Procedures for Steel Pipelines Using a Modified Reference Stress Solution, ASME Journal of Pressure Vessel Technology 131(3): 031409. https://doi.org/10.1115/1.3122769.
15. **Jia, P. Y.; Jing, H. Y.; Xu, L. Y.; Han, Y.; Zhao, L.** 2017. A modified fracture assessment method for pipelines under combined inner pressure and large-scale axial plastic strain, Theoretical and Applied Fracture Mechanics 87: 91-98. https://doi.org/10.1016/j.tafmec.2016.10.007.
16. **Li, Y. Z.; Gong, B. M.; Lacidogna, G.; Carpinteri, A.; Wang, D.** 2019. An improved crack driving force estimation approach for stress-based engineering critical assessment of reeled pipes, Theoretical and Applied Fracture Mechanics 103: 102312. https://doi.org/10.1016/j.tafmec.2019.102312.
17. **Zhang, Y. L.; Hou, R. G.; Wang, R.; Zhang, M; Lyu, Z.** 2023. Three-dimensional model reconstruction of pipeline with inner wall corrosion based on ultrasonic phased array technology, Oil & Gas Storage and Transportation 42(12): 1369-1375. Available at: https://yqcy.pipechina.com.cn/en/article/doi/10.6047/j.issn.1000-8241.2023.12.006.
18. **Yang, Y.; Zhang, H.; Wu, K.; Chen, P.; Sui, Y.; Yang, D.; Liu, X.** 2021. Strain capacity analysis of the mismatched welding joint with misalignments of D 1,422 mm X80 steel pipelines: An experimental and numerical investigation, Journal of Pipeline Science and Engineering 1(2): 212-224. https://doi.org/10.1016/j.jpse.2021.05.002.
19. **Fajuyigbe, A.; Brennan, F.** 2021. Fitness-for-purpose assessment of cracked offshore wind turbine monopile, Marine Structures 77: 102965. https://doi.org/10.1016/j.marstruc.2021.102965.
20. **Liu, Y. Q.; Zhang, Z. Y.; Wu, S. S.; Ji, B.; Zhang, H.; Liu, X.** 2023. Safety assessment on girth welds of large-diameter X80 pipelines in water network area, Oil & Gas Storage and Transportation 42(10): 1128-1136. Available at: https://yqcy.pipechina.com.cn/en/article/doi/10.6047/j.issn.1000-8241.2023.10.006.
21. **Ainsworth, R. A.** 1984. The assessment of defects in structures of strain hardening material, Engineering Fracture Mechanics 19(4): 633-642. https://doi.org/10.1016/0013-7944(84)90096-1.
22. **Kim, S. H.; Han, J. J.; Kim, Y. J.** 2014. Limit Load Solutions of V-groove Welded Pipes with a Circumferential Crack at the Centre of Weld, Procedia Materials Science 3: 706-713. https://doi.org/10.1016/j.mspro.2014.06.116.
23. **Hong, Y.** 2023. Research on the Effect of Indentation Deformation on the Applicability of Girth Weld of Pipeline with Crack, China University of Petroleum. Beijing. https://doi.org/10.27643/d.cnki.gsybu.2023.000763.
24. **Jayadevan, K. R.; Østby, E.; Thaulow, C.** 2004. Fracture response of pipelines subjected to large plastic deformation under tension, International Journal of Pressure Vessels and Piping 81(9): 771-783. https://doi.org/10.1016/j.ijpvp.2004.04.005.
25. **Wu, K.; Zhang, D.; Feng, Q. S.; Yang, Y.; Dai, L. S.; Wang, D. Y.; Zhang, H.; Guo, G. F.; Liu, X.B.** 2023. Improvement of fracture assessment method for pipe girth weld based on failure assessment diagram, International Journal of Pressure Vessels and Piping 204: 104950. https://doi.org/10.1016/j.ijpvp.2023.104950.
26. **Jia, P. Y.; Jing, H. Y.; Xu, L. Y.; Han, Y. D.; Zhao, L.** 2016. A modified reference strain method for engineering critical assessment of reeled pipelines, International Journal of Mechanical Sciences 105: 23-31. https://doi.org/10.1016/j.ijmecsci.2015.11.003.
27. **Wang X.; Shuai, J.; Zhang, S. Z.; WANG, R.; Duo Y.** 2023. A strain based failure assessment method for girth welded joints in high grade steel line pipes, Natural Gas Industry 43(2): 121-130. https://doi.org/10.3787/j.issn.1000-0976.2023.02.012.
28. CSA Z662:19 Oil and gas pipeline systems. National Standard of Canada. 923p.
29. **Kim, Y. J.; Budden, P. J.** 2002. Reference Stress Approximations for *J* and COD of Circumferential Through-Wall Cracked Pipes, International Journal of Fracture 116: 195-218. https://doi.org/10.1023/A:1020158730727.

X.T. Wu, H. Zhang, S.S. Wu, P.C. Chen, H. Wang, X.B. Liu

ENHANCING FRACTURE ASSESSMENT OF PIPE GIRTH WELDS WITH ROOT CRACKS

S u m m a r y

Despite the widespread use of the failure assess–ment diagram, accurately evaluating girth weld joints with cracks remains a significant challenge within the pipeline industry, due to the mismatched strength between the parent metal and weld metal. To Address this issue, an innovative approach was proposed by converting the heterogeneous girth welds as an equivalent homogeneous structure and deriving an equivalent stress-strain relation, thereby enabling the construction of a failure assessment curve for girth welds. This study aims at enhancing the precision of defect assessment in girth welded joints. Firstly, a finite element model is developed to characterize the crack driving force in high-grade pipeline girth welds. Furthermore, an optimized calculation method is proposed for determining the reference stress and limit load of pipeline girth welds with root cracks by introducing a correction factor. Moreover, a predictive formula for the correction factor has been established based on finite element simulation results. Through rigorous numerical simulations and methodical calculation techniques, this study aims to provide guidance for the accurate evaluation of girth weld root cracks in pipeline engineering applications.

Keywords: pipe girth weld, root cracks, fracture assessment, failure assessment diagram.

Received June 30, 2024
Accepted June 25, 2025